The NaxMoO2 phase diagram ($1/2 \leq x < 1$): an electrochemical devil's staircase

Laura Vitoux, Marie Guignard, Matthew R. Suchomel, James C. Pramudita, Neeraj Sharma, Claude Delmas

The Na_xMoO_2 Phase Diagram ($1/2 \leq x < 1$): An Electrochemical Devil's Staircase

Laura Vitoux[1,2], Marie Guignard[1,2]*, Matthew R. Suchomel[1,2], James C. Pramudita[3], Neeraj Sharma[3], Claude Delmas[1,2]

[1] CNRS, ICMCB, 87 avenue du Dr A. Schweitzer, 33608 Pessac Cedex, France, [2] Université de Bordeaux, ICMCB, 87 avenue du Dr A. Schweitzer, 33608 Pessac Cedex, France. [3] School of Chemistry, UNSW Australia, Sydney, New South Wales 2052, Australia.

ABSTRACT: Layered sodium transition metal oxides represent a complex class of materials that exhibit a variety of properties, e.g. superconductivity, and can feature in a range of applications, e.g. batteries. Understanding the structure-function relationship is key to developing better materials. In this context, the phase diagram of the Na_xMoO_2 system has been studied using electrochemistry combined with *in situ* synchrotron X-ray diffraction experiments. The many steps observed in the electrochemical curve of $Na_{2/3}MoO_2$ during cycling in a sodium battery suggests numerous reversible structural transitions during sodium (de)intercalation between $Na_{0.5}MoO_2$ and $Na_{\sim 1}MoO_2$. *In situ* X-ray diffraction confirmed the complexity of the phase diagram within this domain, thirteen single phase domains with minute changes in sodium contents. Almost all display superstructure or modulation peaks in their X-ray diffraction patterns suggesting the existence of many Na_xMoO_2 specific phases that are believed to be characterized by sodium/vacancy ordering as well as Mo-Mo bonds and subsequent Mo-O distances patterning in the structures. Moreover, a room temperature triclinic distortion was evidenced in the composition range $0.58 \leq x < 0.75$, for the first time in a sodium layered oxide system. Monoclinic and triclinic subcell parameters were refined for every Na_xMoO_2 phase identified. Reversible $[MoO_2]$ slab glidings occur during the sodium (de)intercalation. This level of structural detail provides unprecedented insight on the phases present and their evolution which may allow each phase to be isolated and examined in more detail.

1. INTRODUCTION

Sodium layered oxides Na_xMO_2 (M: transition metal, x: sodium content) are being revisited for their potential use as positive electrode materials in sodium-ion batteries for stationary energy storage. This family of compounds composed of $[MO_2]$ slabs with Na^+ ions inserted in the interslab space, can also feature interesting physical properties and thus are of signfiicant interest in the search of new electron correlated materials[1–11]. Notably, the interaction between the sodium and sodium vacancy ordering (whether it is commensurate or not) and the possibility of charge ordering in the $[MO_2]$ layers lead to peculiar cationic distributions within the $[MO_2]$ layers. In order to describe the complex relationship existing in these materials between structure, chemical composition (nature of the transition metal, sodium content) and the physical properties, several systems have to be investigated. Exploring new systems would involve synthesizing each composition and characterizing its structure, however, an alternative and possibly efficient method to characterize phase diagrams is the use of electrochemistry to change the alkali ion content and hence M oxidation state while simultaneously collecting structural data[12]. The result of which is a map of the phase diagram of the Na_xMO_2 systems studied under the electrochemical conditions employed. [6,9,10,13].

The Na_xMoO_2 system is particularly interesting because molybdenum (d^2 and d^3) is well-known for its tendency to form Mo-Mo bonds. This behavior was observed in several molybdenum oxides in which the molybdenum oxidation state is smaller than 4 [14–20]. Mo-Mo bonds are therefore expected to form in the $[MoO_2]$ slabs of the Na_xMoO_2 phases alongside sodium/vacancy ordering and can have a dramatic effect on the properties of the materials.

To date, only three phases $Na_{2/3}MoO_2$, $Na_{1/2}MoO_2$ and $NaMoO_2$ have been studied. The solid state synthesis of $Na_{2/3}MoO_2$ was first reported in the 60s without any structural characterization [21,22]. Cell parameters for this compound were determined in 1984 from single crystal X-ray diffraction experiments [23]. The electrochemical investigation of the Na_xMoO_2 system using $Na_{2/3}MoO_2$ as a positive electrode material in a sodium battery [24] revealed a reversible sodium intercalation in Na_xMoO_2 in the composition domain $0.28 < x < 0.95$. The complex nature of the electrochemical curve suggests many structural transitions during (de)intercalation. From an *in situ* X-ray diffraction experiment performed at different fixed electrochemical cell voltages, i.e. to isolate different Na_xMoO_2 compositions, five single-phase domains were distinguished in this sodium composition range. However, the phase diagram is clearly more complicated judging by the multi-step nature of the electrochemical curve within and around these five domains. No

structural models have been proposed for any of these de-intercalated Na_xMoO_2 phases apart from cell parameters for $Na_{1/2}MoO_2$. In parallel, a structure for $Na_{1/2}MoO_2$ was proposed from single crystal X-ray diffraction, in which sodium occupies octahedral sites between the $[MoO_2]$ slabs containing Mo-Mo zig-zag bonds[14]. The stability of this arrangement has been studied in the frame of theoretical investigation of transition metal dioxides in 1985 [25]. Mo-Mo bonds are also thought to exist in the fully intercalated phase $NaMoO_2$ to explain its low paramagnetism[26]. The structures of the numerous Na_xMoO_2 phases, whose existence is suggested by the electrochemical curve, can therefore be expected to differ from one another by various arrangements of Mo-Mo bonds as well as sodium/vacancy orderings.

In this work, we investigate the Na_xMoO_2 system ($1/2 \leq x < 1$) by combining electrochemistry in a sodium battery and *in situ* X-ray powder diffraction in order to determine the phase diagram and characterize precisely the structural transitions occurring upon sodium (de)intercalation. In particular, we aim at identifying specific compositions at which we assume the existence of sodium/vacancy ordering and/or Mo-Mo bonding.

2. EXPERIMENTAL SECTION

2.1 Synthesis

The starting material Na_xMoO_2 was obtained by the solid state synthesis using a stoichiometric target of $Na_{2/3}MoO_2$[22,24]. Na_2MoO_4 was obtained by dehydration of Na_2MoO_4, $2H_2O$ (VWR, 98%). Na_2MoO_4, MoO_2 (Sigma Aldrich, 99%) and Mo (VWR, 99.9%) in stoichiometric amounts were ball-milled (400 rpm/min for 3 h) and heated in a sealed gold tube with argon at 700 °C for 90 h. The resulting material, a well crystallized black powder, was recovered in a glovebox under argon atmosphere to prevent oxidation and reaction with air moisture.

2.2 X-ray powder diffraction

Preliminary laboratory based X-ray powder diffraction measurements (Cu-source Panalytical X'Pert Pro) were performed on $Na_{2/3}MoO_2$ samples in sealed glass capillaries (0.2 mm diameter). High resolution X-ray powder diffraction data for $Na_{2/3}MoO_2$ were collected at the 11-BM beamline of the Advanced Photon Source (APS) at Argonne National Laboratory using an average wavelength of 0.41417(2) Å. Discrete detectors covering an angular range from -6 to 16 ° were scanned over a 34 ° 2θ-range, with data points collected every 0.001 ° and scan speed of 0.01°/s. The powder was loaded in sealed 0.8 mm diameter capillaries. Profile refinement using the Le Bail method was carried out using the JANA2006 program[27].

2.3 Electrochemical characterization

Electrochemical characterization was undertaken in 2032 type coin cells with the following electrochemical arrangement: Na | $NaClO_4$ in PC (1M) | $Na_{2/3}MoO_2$ mixed with graphite + carbon black powder (Strem Chemicals) and PTFE (polytetrafluoroethylene) as binder (88: 10: 2 weight ratio). The batteries were assembled in glove boxes and cycled using a Biologic VMP3 potentiostat at 25 °C in a temperature-controlled room. Galvanostatic cycling was performed at C/100 rate (1 Na^+ per formula unit (de)intercalated in 100 h) between 2.5 V and 0.8 V. Galvanostatic Intermittent Titration Technique (GITT) mode was also used in the voltage range $0.7 \leq V \leq 2.2$, where 15-minute discharge at C/100 rate were alternated with 3-hour relaxation periods during which no current was applied.

2.4 *In situ* X-ray powder diffraction

Two complementary *in situ* X-ray diffraction experiments were undertaken at different synchrotron facilities to follow the structural evolution of the Na_xMoO_2 material at the positive electrode during the discharge of a sodium battery with the same electrochemical arrangement as above. X-ray diffraction experiments were performed in transmission mode meaning that the X-ray beam go through the electrochemical cell. The sodium batteries were in these cases assembled in modified coin cells to allow penetration and limit the strong contribution to the X-ray diffraction patterns of the cell components other than the Na_xMoO_2 positive electrode. Small (~3 mm diameter) openings were pierced in the modified coin cells and covered by gastight sealed Kapton windows to increase X-ray transmission. The positive electrode current collector made of a thin stainless steel or aluminum foil was used to ensure a high X-ray beam transparency while maintaining good electronic contact with the entire electrode. Finally, a thin foil of Na metal (~200 µm) was used as the negative electrode. Nevertheless, some diffraction from the *in situ* cell components, mainly from the stainless steel and the aluminum used in the current collectors, can still be seen on the collected X-ray diffraction patterns and are marked by the "§" symbol in the results section. In both *in situ* X-ray diffraction experiments, 4 cells were cycled at the same time on a carousel and placed in front of the beam at regular intervals for data acquisition.

The first experiment, undertaken at the 11-BM beamline at the APS was performed in *operando* mode. The cell was previously charged to 2.5 V vs Na^+/Na corresponding to $Na_{1/2}MoO_2$ and then continuously discharged to 0.9 V corresponding to $Na_{\sim 1}MoO_2$ at C/100 rate without relaxation times. X-ray diffraction data were collected between 1° and 28° (λ = 0.41373(2) Å) for 15 minutes every hour (equal to a step of 0.01 Na per formula unit between each pattern).

The second experiment, undertaken at the Australian Synchrotron, was performed in *in situ* mode, in a restrained range of composition ($0.57 < x < 0.77$). The cell was previously charged to 2.1 V vs Na^+/Na corresponding to $Na_{\sim 0.57}MoO_2$ and then discharged until 1.0 V ($Na_{0.77}MoO_2$) in GITT mode alternating with 6 min discharge at C/28 rate (0.0357 Na^+ per formula unit deintercalated in 1h) and 14 min relaxation periods. X-ray diffraction measurements (λ = 0.68807(2) Å) were recorded between 4° and 84° during the last 4 minutes of the relaxation period when the voltage is virtually stabilized and the material close to the equilibrium.

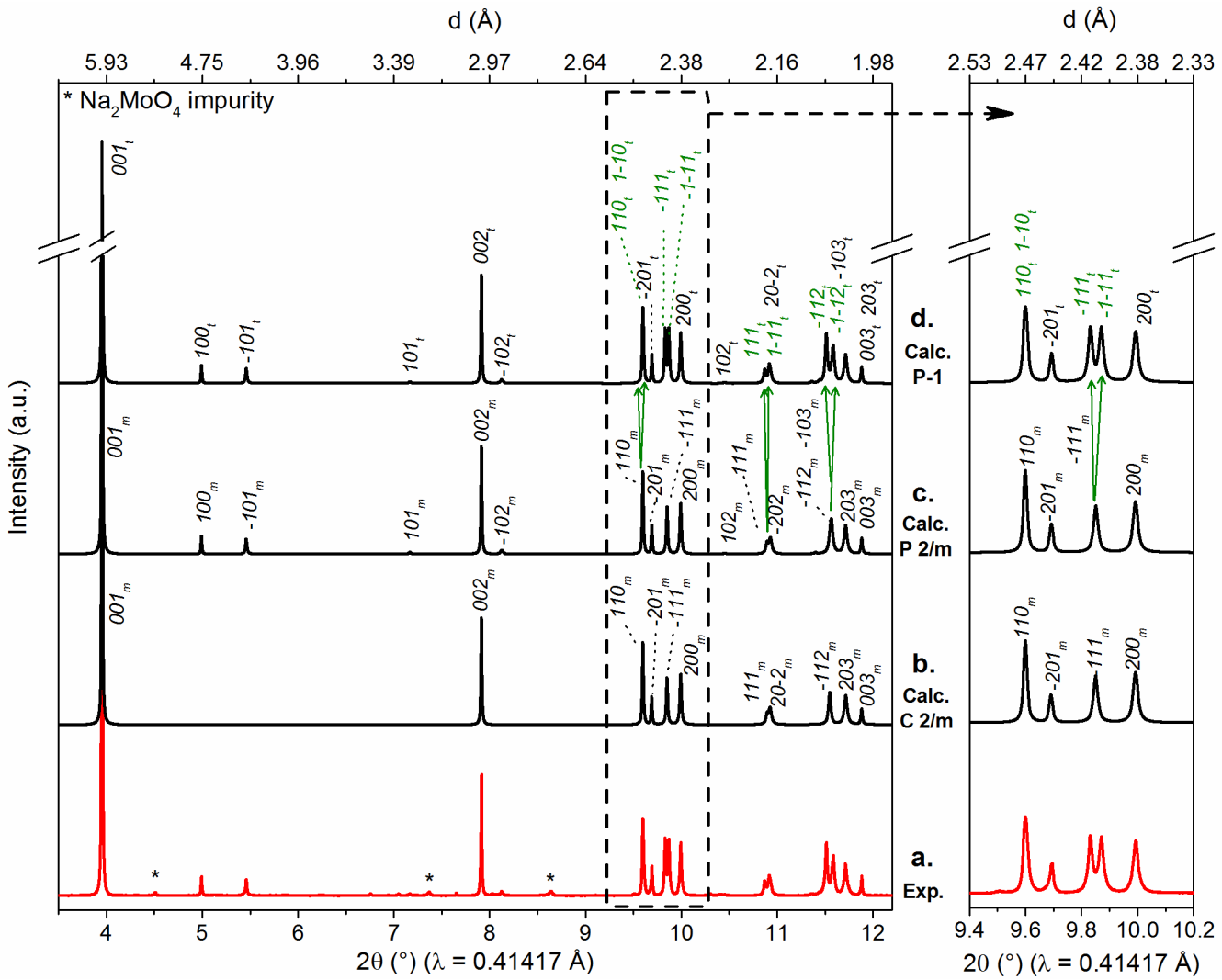

Figure 1. Experimental synchrotron X-ray powder diffraction pattern of $Na_{2/3}MoO_2$ (red line) compared to the calculated patterns using different cells (black lines). Bragg indexations resulting from the triclinic distortion in green.

3. RESULTS AND DISCUSSION

3.1 Pristine material synthesis and structural characterization

The pristine material was obtained from the solid-state synthesis reported in the literature[22,24] targeting the $Na_{2/3}MoO_2$ composition, which consists in reacting Na_2MoO_4, MoO_2 and Mo powders at 700°C for 90h. Preliminary characterization using lab X-ray diffraction revealed the presence of small amounts of Na_2MoO_4 and Mo impurities. Several synthesis experiments were then performed to optimize the initial stoichiometry, the temperature (600°C – 900°C) and the duration of the thermal treatment Synthesis tests with slightly less initial Na_2MoO_4 reagent had little effect on the final amount of Na_2MoO_4 in the resulting material. Thermal treatments at temperatures above 700°C lead to the formation of a secondary unknown phase, in addition to Na_2MoO_4 and Mo. The best synthesis conditions were therefore found to be the ones reported in the literature[22,24] (700 °C, 90 h). The Na_2MoO_4 and Mo impurities in these materials are considered in negligible amounts for our further investigations. They are believed to result from the disproportionation of the layered material at high temperature: it was found, experimentally and in the literature[21,22], that Na_2MoO_4 forms during the synthesis of the Na_xMoO_2 phase even when it is not used as a reactant. The presence of these impurities implies a small deficit of sodium vs the targeted $Na_{2/3}MoO_2$ composition and prevents the direct determination of the sodium content in the layered oxide phase by induced coupled plasma-atomic emission spectroscopy analysis (ICP).

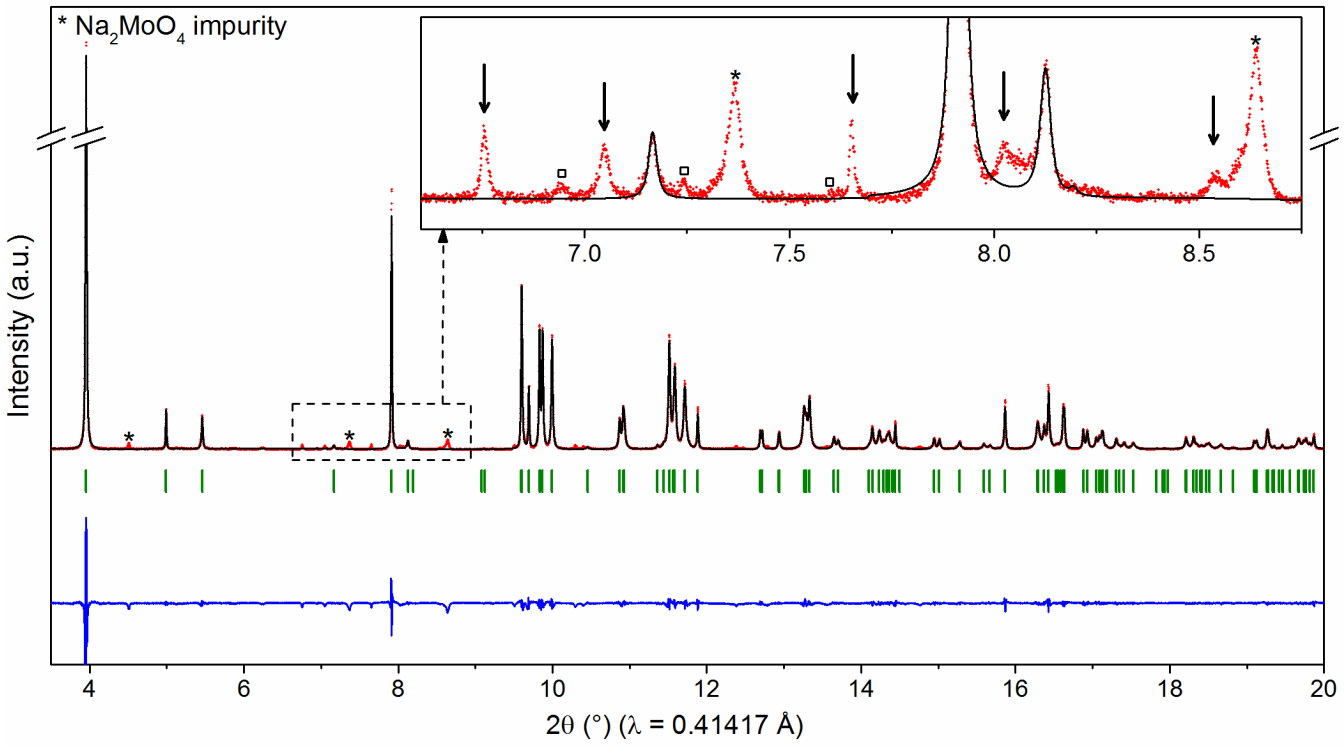

Figure 2. Experimental synchrotron powder diffraction pattern of the starting material $Na_{2/3}MoO_2$ (red diamonds) and calculated profile by the Le Bail refinement (χ^2 = 2.43, Rp = 9.01 %, Rwp = 12.79 %) using the following triclinic cell : a = 4.9424(1) Å, b = 2.8985(3) Å, c = 6.2385(2) Å, α = 90.394(2)°, β = 105.820(3)°, γ = 89.933(2)° (black line) . The difference is drawn in blue and Bragg reflections are stated by green ticks. Superstructure peaks are shown by arrows in the insert. Squares state the reflections of an unknown impurity.

Given the complexity of the X-ray powder diffraction pattern for the $Na_{2/3}MoO_2$ phase, structural characterization was performed using high resolution X-ray powder diffraction (**Figure 1a**). Profile refinement using the Le Bail method were first performed without success using the monoclinic lattice parameters reported for single crystals of $Na_{2/3}MoO_2$[23]. The inadequacy of these published parameters to index our experimental data is thought to result from the significant differences in the stoichiometry between the single crystals and the powder sample.

It should be noted, that no precautions were taken in handling the single crystal products, which are likely to react in ambient atmospheres. A new unit cell was therefore needed to index the experimental powder data. The experimental X-ray diffraction pattern was found to have similarities with the patterns of O'3-Na_xMO_2 compounds which crystallize in the C2/m monoclinic space group [10,28–32]. According to this structural model, the most intense peak at low 2θ corresponds to the 001_m Bragg reflection, and three of the five reflections between 2θ = 9.5 ° and 2θ = 10.2 ° are indexed with 110_m, -201_m and 200_m Bragg reflections. Various permutations for indexing were trialed but the best indexing was found for a monoclinic cell whose parameters are a = 4.9332(5) Å, b = 2.8884(3) Å, c = 6.2391(8) Å, β = 105.85(1) °. Although most of the reflections are indexed in this model, a few differences can be observed between the experimental and calculated diffraction patterns in this cell (space group C2/m) (**Figure 1b**). Several low intensity reflections are not indexed in this cell, such as the two peaks at 2θ = 5 ° and 2θ = 5.45 °, and the two peaks observed in the experimental pattern instead of the single calculated peak for the $-11l_m$ Bragg reflections at 2θ = 9.85° and 2θ = 11.55° . First, the symmetry restrictions of the C2/m space group could induce the extinctions of some Bragg reflections. Choosing the monoclinic P2/m space group, which does not impose any specific conditions on the *hkl* as shown in **Figure 1c**, results in all the reflections to be indexed in this new cell except for the split peaks corresponding to the $-11l_m$ Bragg reflections. The angles were then allowed to refine in the triclinic space group P-1 (**Figure 1d**). A slight difference (< 1°) from 90° of both α and γ angles was sufficient to explain the splitting of the monoclinic $-11l_m$ peak into the two peaks observed in the experimental patterns and are thus indexed respectively as $-11l_t$ and $-1-1l_t$. The cell parameters were refined using this triclinic cell and the corresponding profile refinement using the Le Bail method is presented in **Figure 2.** The resulting refined cell parameters are a = 4.9424(1) Å, b = 2.8985(3) Å, c = 6.2385(2) Å, α = 90.394(2) °, β = 105.820(3) °, γ = 89.933(2) °. In the triclinic cell all the intense diffraction lines are indexed except for peaks of low intensity highlighted by arrows on the enlargement of the X-ray diffraction pattern between 6.5 ° and 8.6 ° (**insert Figure 2**).

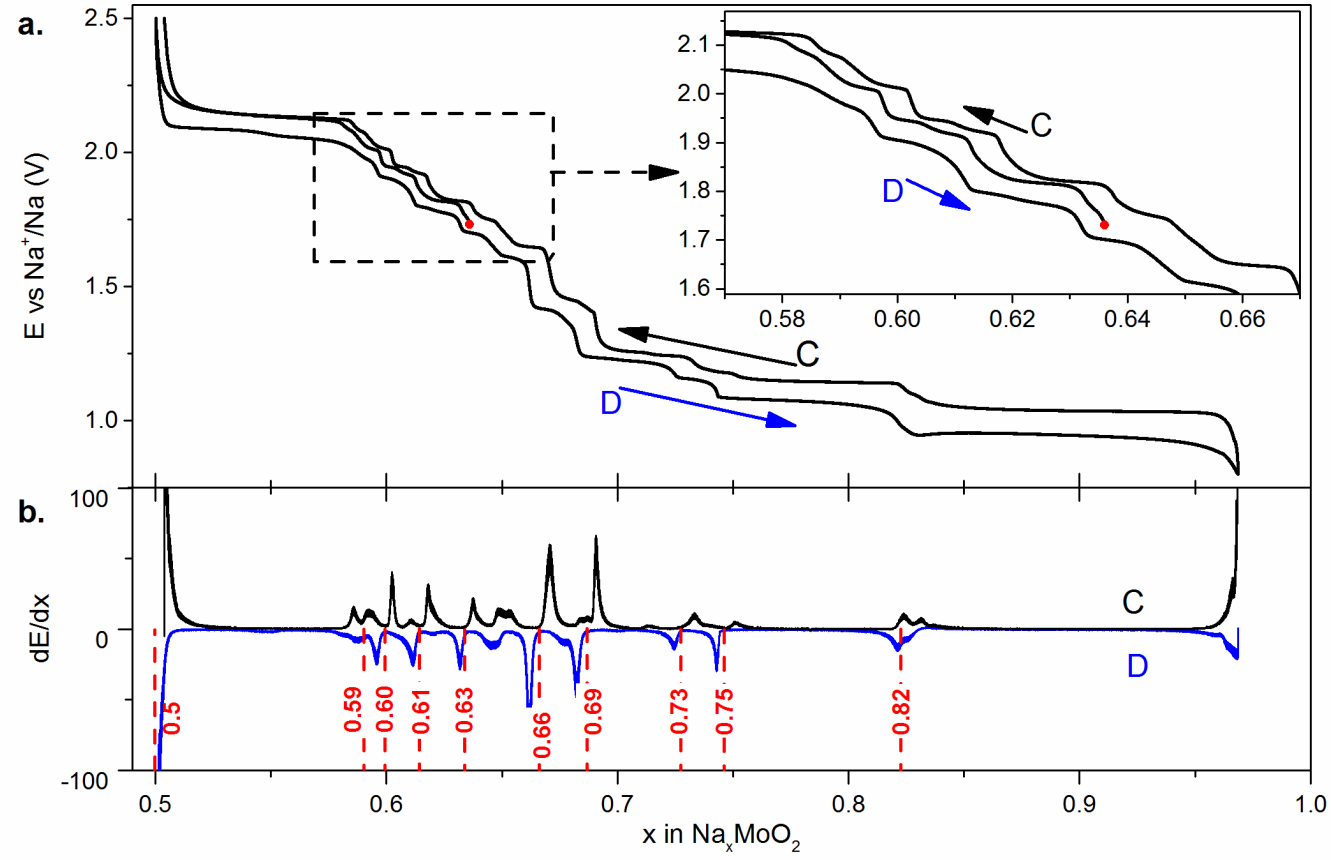

Figure 3. a. First galvanostatic cycle (C: Charge, D : Discharge) of the electrochemical cell between $Na_{0.5}MoO_2$ and $Na_{\sim 0.97}MoO_2$. Initial voltage is marked by a red dot. b. dE/dx derivative curve.

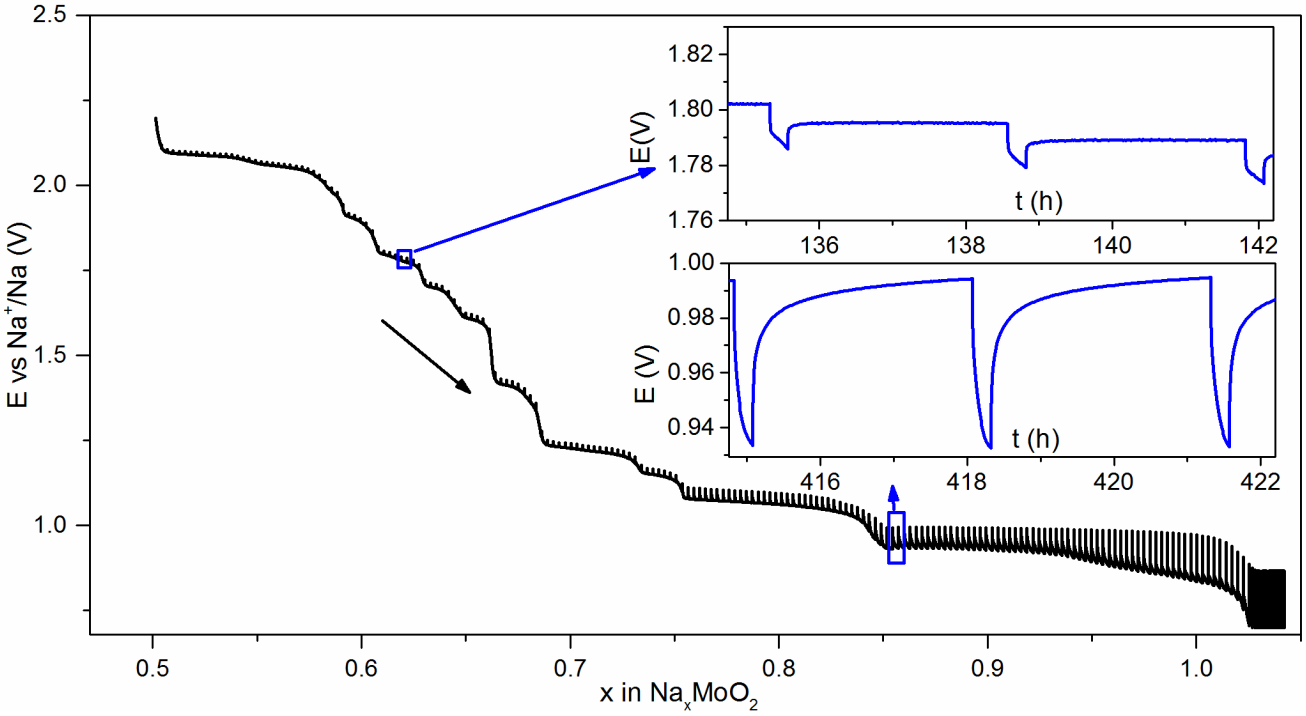

Figure 4. First discharge in GITT mode of the electrochemical cell between $Na_{0.5}MoO_2$ and $Na_{\sim 1}MoO_2$.

They imply the existence of a superstructure resulting from sodium/vacancy ordering and/or molybdenum displacement within the [MoO_2] layers. The determination of the superstructure, which is still under progress, is essential to perform a reliable refinement of the structure by the Rietveld method.

3.2 Electrochemical characterization

In order to illustrate the phase diagram of the Na_xMoO_2 system, the $Na_{2/3}MoO_2$ was used as a positive electrode in a sodium battery.The cell was cycled at very low rate C/100 (1 Na deintercalated in 100 h) between 2.5 V and 0.8 V to ensure a near-equilibrium state between $Na_{1/2}MoO_2$ and $Na_{\sim 1}MoO_2$. The multi-step nature of the corresponding electrochemical curve, presented in **Figure 3a**, suggest numerous structural transitions in agreement with the observations reported in the literature[24].

In most of the other Na_xMO_2 systems (M = Co, V, Cr, Ni...) reported in the literature[6,9,10,33–36], the most important voltage drops occur for the $Na_{1/2}MO_2$ and $Na_{2/3}MoO_2$ compositions which are energetically favorable for sodium/vacancy ordering. The initial sodium content in the starting material Na_xMoO_2 is therefore reevaluated by fitting the 2.5 V and 1.5 V voltage drops at x= 1/2 and 2/3, respectively. It is usually slightly lower than the target composition ($x \approx 0.63$) and it varies subtly from one synthesis to another.

The structural transitions are reversible as the charge curve is distinctly similar to the first discharge curve and displays the same voltage variations. Significantly better resolution is afforded in this work compared to the previously reported study[24] in particular for sodium contents x between ~ 0.57 and 2/3 as shown in the **insert of Figure 3a**. Interestingly it displays several potential drops, for close sodium contents, highlighted by sharp peaks on the derivative curve dE/dx as function of x in Na_xMoO_2 **Figure 3b**. They are characteristic of single phases with a defined composition at which sodium/vacancy ordering in the interslab region and/or Mo patterning in the [MoO_2] slabs are believed to exist.

Sodium content at the equilibrium of the specific phases can be deduced from the average between the values on the charge and discharge curves and are indicated in red on the derivative curve (**Figure 3b**). Ten specific phases are observed: x = 0.50, 0.59, 0.60, 0.61, 0.63, 0.66, 0.69, 0.73, 0.75, 0.82. Specific phases are separated from one another by a biphasic domain stated by a voltage plateau as seen at high sodium content ($0.75 < x < 0.95$). For sodium content $x < 0.75$, however, the type of behavior between specific phases is less clear because of the restricted domain of composition concerned.

A Galvanostatic Intermittent Titration Technique (GITT) discharge was undertaken in order to study more precisely the material close to the thermodynamic equilibrium (**Figure 4**). It consists of alternating discharge (15 minutes at C/100) with relaxation periods (3 hours) during which no current is applied and thus the material homogenizes with respect to voltage. In the insert, one can see that in the $0.5 < x < 0.75$ composition domain, intercalation kinetics are rapid as the polarization is minute and the equilibrium (stable voltage) is obtained after less than 1 h. This suggests a high ionic and electronic conductivity in this composition range. Relaxation times and polarization clearly increase for high sodium contents ($x > 0.75$) and may be explained by lower ionic conductivity. Indeed, at high sodium contents, most of the interstitial sites are occupied, intuitively making the sodium mobility from one site to an empty site more difficult. In this composition range, there is furthermore the possible degradation of the liquid electrolyte. These factors induce an overestimation of the sodium content at low voltage which is particularly noticeable at the end of intercalation ($x > 1$).

3.3 *In situ* X-ray powder diffraction

The short relaxation times in the most complex section of the GITT discharge curve enable *in situ* X-ray diffraction studies to continuously probe the structural transitions during the electrochemical intercalation of sodium. A phase diagram can then be determined by differentiating monophasic domains (solid solution) and biphasic domains. In a solid solution domain, the distance between the center of two successive [MoO_2] slabs (termed the interslab distance), which is directly correlated to the position of the *00l* reflections in the X-ray diffraction patterns and is shown to vary continuously with the sodium amount. As soon as there is an ordering, there is a structural relaxation leading to a discontinuity in the interslab distance variation, in addition to the appearance of unindexed reflections of low intensity at low 2θ angles. Cation distribution can be commensurate or incommensurate with respect to the initial structure, leading then to superstructure or modulation peaks. The variation of the width and intensity of the *00l* peak is also a very good indicator of the existence of biphasic domains. As shown for the Na_xCoO_2 system[6], a broadening of the *00l* reflection in a narrow composition domain indicates the presence of two reflections with very close *d*-spacings (~interslab distance), in other words characteristic of a biphasic domain. When the difference in *d*-spacings is greater, both *00l* diffraction lines appear distinctively simultaneously on the X-ray patterns and typically one increases while the other decreases in intensity over the course of the biphasic region.

Operando in situ X-ray diffraction ($1/2 \leq x \leq 1$)

An *in situ operando* X-ray diffraction experiment was carried out to provide a general overview of the structural rearrangements occurring in Na_xMoO_2 upon sodium intercalation between $Na_{1/2}MoO_2$ and $NaMoO_2$ (see Experimental section). The X-ray diffraction patterns recorded during the discharge from the $Na_{1/2}MoO_2$ composition are shown in **Figure 5**. Despite the close step size in sodium content (Δx = 0.01 Na) imposed between each X-ray diffraction measurement, the differences between each pattern are significant. Nevertheless, all present common features suggesting that the general structure is preserved.

All X-ray diffraction patterns collected during the X-ray diffraction experiments are indexed in their common monoclinic or triclinic subcell, which indexed the main diffraction reflections but not the superstructure or modulation peaks at low 2θ.

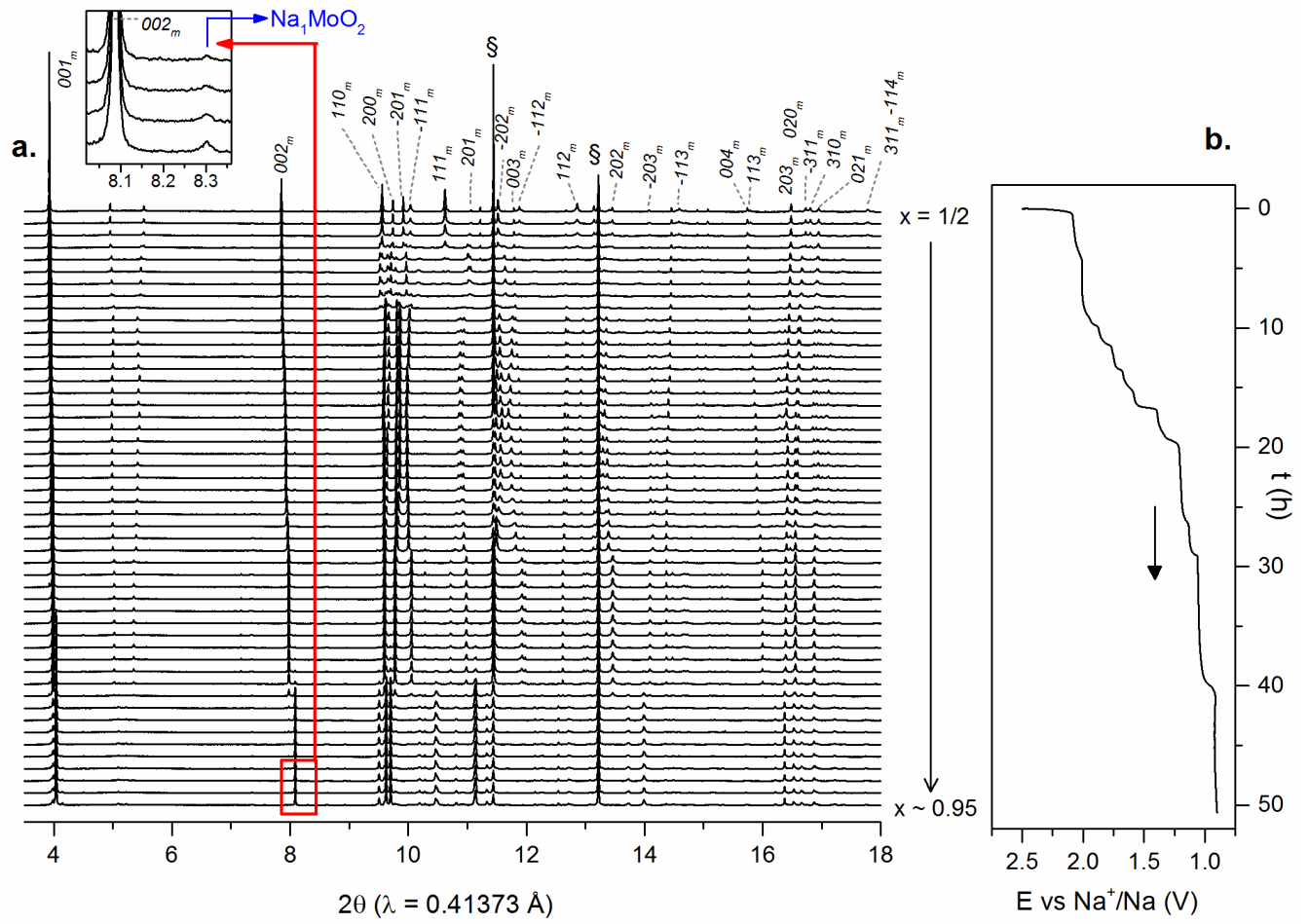

Figure 5. a. Synchrotron powder diffraction patterns recorded during the operando in situ X-ray diffraction experiment. Bragg indexation of the $Na_{1/2}MoO_2$ phase (top pattern) in the initial monoclinic subcell are indicated. « § » states to the reflections of the stainless steel constituting the in situ cell. b. Electrochemical curve recorded during the operando in situ experiment.

The triclinic cell (P-1 space group) determined previously for the indexation of the pristine material $Na_{2/3}MoO_2$ is used as a common subcell to all the X-ray diffraction patterns in the triclinic range. The corresponding common monoclinic subcell is deduced by fixing the α and γ at 90°. In Figure 5, only the monoclinic indexation for $Na_{1/2}MoO_2$ is reported.

Critical shifts of the *-201m*, *200m* and *-110m* reflections compared to *002m* and *110m* reflections and a change in intensities between $Na_{0.5}MoO_2$ and $Na_{0.60}MoO_2$ is noted. This suggests an important structural rearrangement, which could lead to the formation of stacking faults and therefore explains the broadening of the diffraction lines in this composition range. Although the *001* and *002* reflections are very narrow for the composition x ≈ 0.55, suggesting a single phase for this composition, the number of reflections in the 9.4-10.8° 2θ-range is too large to be indexed by the common subcell. Therefore, although we think that a single phase exists for x ≈ 0.55, we could not index its unit cell from our operando experimental diffraction data.

From $Na_{0.60}MoO_2$, X-ray diffraction patterns are again well-defined, and a splitting of the peaks *110m* and *-111m* can be seen between $Na_{0.60}MoO_2$ and $Na_{0.75}MoO_2$. As previously demonstrated for the pristine material $Na_{2/3}MoO_2$, the splitting of these peaks is the result of a triclinic distortion of the cell (α ≈ 90.4° and γ ≈ 89.8°). Patterns in this domain of composition are indexed in the triclinic space group P-1. Whereas monoclinic distortion is common in sodium layered oxides, it is to the best of our knowledge the first time that a triclinic distortion is evidenced in layered oxides at room temperature. It can therefore be associated with the presence of molybdenum in the structure and more precisely to the existence of specific Mo patterning in the $[MoO_2]$ slabs.

The triclinic distortion comes with an important and complicated shifting of the reflections. Moreover, numerous satellite peaks, appearing between 6° and 7.8°, are not indexed in the initial subcell. Therefore, several ordered Na_xMoO_2 phases characterized by different superstructures or modulated structures, resulting from sodium/vacancy ordering and/or the formation of Mo-Mo bonds, probably exist in this composition domain. However, the sodium step Δx = 0.01 Na per formula unit, and cycling in *operando* mode, do not enable to delimit the domain of existence for each specific phase.

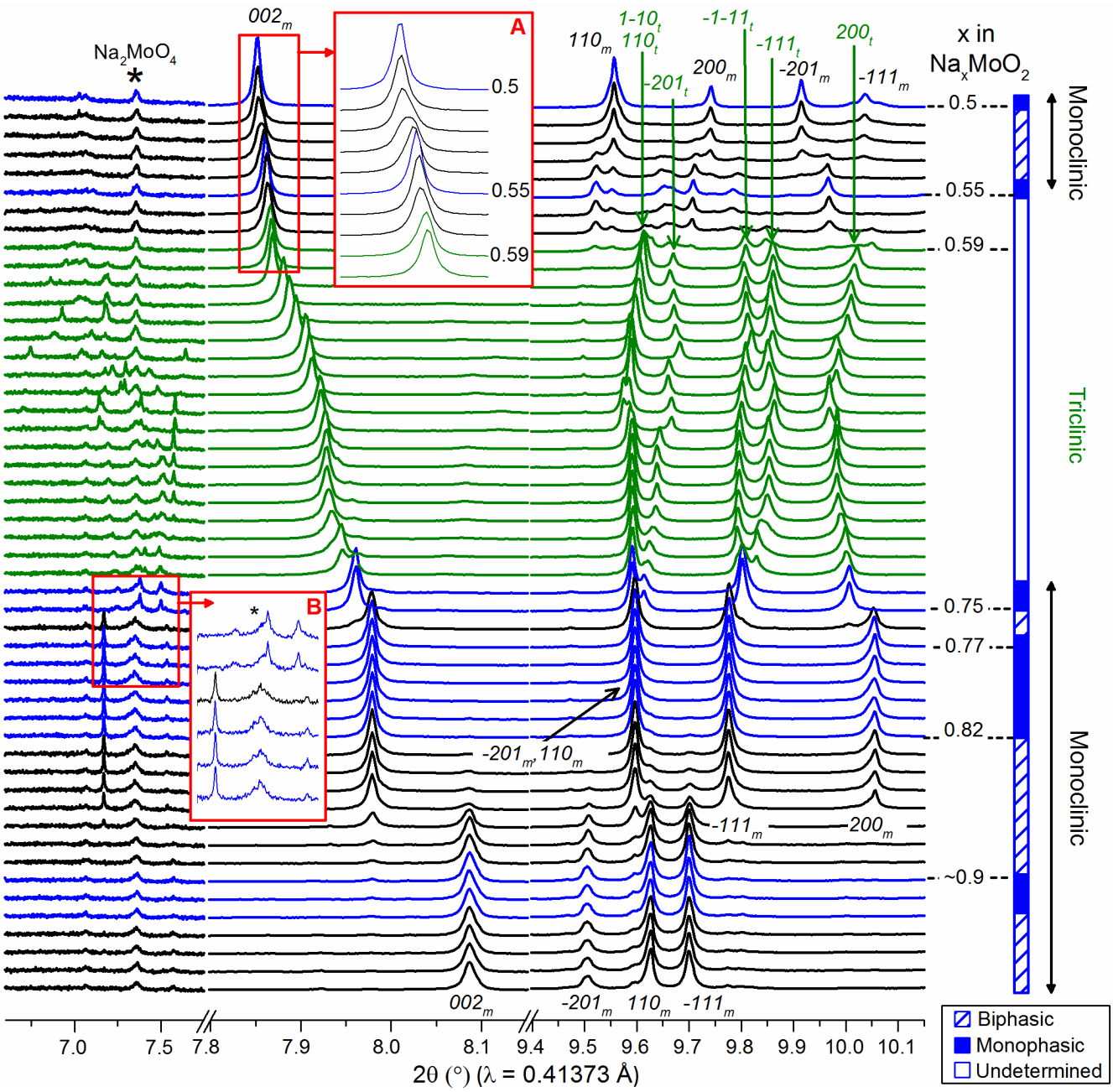

Figure 6. Zoom over the X-ray diffraction patterns collected during the *operando in situ* experiment in the x-range $0.5 \leq x < \sim 0.95$. Bragg indexation in the initial monoclinic cell and triclinic cell are written in black and in green respectively. The phase diagram is presented on the right.

Another *in situ* X-ray experiment (GITT mode) was undertaken to establish the phase diagram specifically in the composition domain where the triclinic distortion occurs (see below). For high sodium contents ($x > 0.75$), *-1-11*$_t$ and *-111*$_t$ converge into a single *-111*$_m$ peak at 9.80° and the X-ray diffraction patterns are again indexed using a monoclinic space group (P2/m). Two monophasic domains around $Na_{0.75}MoO_2$ and Na_xMoO_2 ($0.77 < x < 0.82$) can be distinguished and they are separated by a biphasic domain. In both composition domains, X-ray diffraction patterns feature unindexed reflections at low angles (**insert B Figure 6**). At lower voltage, the reflections of the $Na_{\sim 0.9}MoO_2$ composition appear and become more intense while those of $Na_{0.82}MoO_2$ mostly disappear, indicating the existence of a biphasic domain between these two compositions.

At the end of the discharge, the *00l* reflections of the fully intercalated material Na_1MoO_2 are noted, e.g., see the *002* reflection is shown in **insert Figure 5**. This implies the existence of a last biphasic domain between $Na_{\sim 0.9}MoO_2$ and Na_1MoO_2.

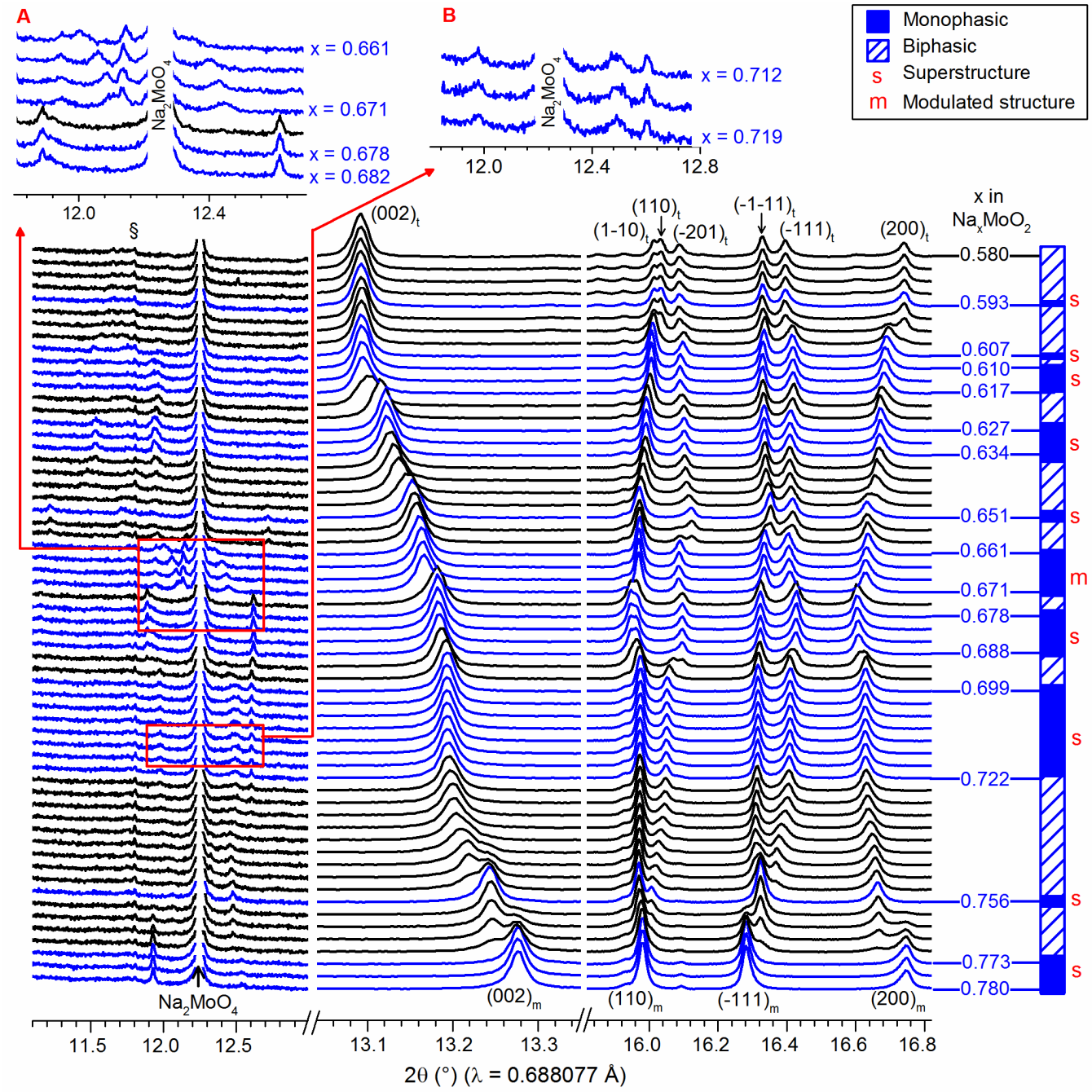

Figure 7. Zoom over X-ray diffraction patterns collected during the *in situ* experiment in the x- range 0.58 ≤ x < 0.78. The detailed phase diagram in the triclinic domain is presented on the right side.

The pure Na_1MoO_2 composition is however not achieved electrochemically because of the low ionic conductivity of this fully intercalated phase and the decomposition of the electrolyte at low voltage, which was previously discussed during the cycling of the cell in GITT mode (**Figure 4**). Electrolyte degradation results, in this experiment, in an extended voltage plateau at ~0.9 V and an overestimation of sodium content for x ≥ 0.82.

In situ X-ray diffraction experiment (0.58 ≤ x ≤ 0.78)

Due to the complex behavior within the range 0.58 < x < 0.78, an *in situ* experiment (GITT mode) was performed at the Australian synchrotron in this restrained range of composition where the triclinic distortion occurs. A smaller sodium step (Δx = 0.0035 per formula unit) between X-ray diffraction measurements was chosen in order to delimit the domain of existence of the several specific Na_xMoO_2 phases displaying satellite peaks. Moreover, these measurements have been made at the end of each relaxation period of the sodium battery, which was cycled in GITT mode. Contrary to *operando* experiments, it enables characterization of the material in the near-equilibrium state and to determine more precisely the sodium content which remains constant during the measurement.

To establish the phase diagram, three parts of the X-ray diffraction patterns are enlarged to focus on the evolution of the same reflections as the previous *operando* experiment (**Figure 7**). Thanks to the smaller sodium step, nine specific compositions or very narrow solid solution domains can be distinguished: $x \approx 0.593$, $x \approx 0.607$, $0.610 \leq x \leq 0.617$, $0.627 \leq x \leq 0.634$, $x \approx 0.651$, $0.661 \leq x \leq 0.671$, $0.678 \leq x \leq 0.688$, $0.699 \leq x \leq 0.722$, $x \approx 0.756$ and $0.773 \leq x \leq \sim 0.82$ (approximated during the previous *operando* X-ray experiment). Using three significant figures e.g., 0.634 in the sodium content has little scientific meaning but are used to easily distinguish each monophasic domain, which are very close in sodium content ($\Delta x < 0.01$). In the rest of the manuscript, only two significant figures will be used. These monophasic domains determined by *in situ* X-ray diffraction are correlated with specific Na_xMoO_2 phases determined on the electrochemical curve by potential drops and on the electrochemical derivative curve by narrow peaks for sodium contents x = 0.59, 0.60, 0.61, 0.63, 0.66, 0.69, 0.73 and 0.75.

It should be noted that the first well resolved X-ray diffraction pattern indexed in a triclinic cell collected in the previous *operando* experiment ($x \approx 0.60$) corresponds in fact to the X-ray diffraction pattern collected in this *in situ* experiment at the sodium content $x \approx 0.61$. The $Na_{\sim 0.59}MoO_2$ triclinic phase corresponds to the intermediate phase, which was thought to exist but not isolated in the previous *operando* experiment. Moreover, X-ray patterns collected during the second *in situ* experiment for sodium contents $0.58 \leq x < 0.59$ feature reflections of very low intensity belonging to the $Na_{0.55}MoO_2$ phase. This confirms the hypothesis of a biphasic domain between these two phases.

Interestingly, X-ray patterns in each of these monophasic domains feature different unindexed reflections, as previously suggested by the o*perando* X-ray diffraction experiment (**Figure 6**). In the narrow composition range $0.66 \leq x \leq 0.67$, the position of the some unindexed reflections shift significantly with the intercalation of sodium compared to the shifting of the reflections indexed in the initial cell (**insert A, Figure 7**). This is characteristic of a incommensurate modulated structure with a modulation vector varying with the sodium content[9,13,37]. For all other compositions, the displacement of the non-indexed reflections relative to the subcell appears to be related to the one of the indexed peaks suggesting the existence of a commensurate superstructure.

Table 1: Refined cell parameters of the specific Na_xMoO_2 phases using the Lebail refinement on the X-ray diffraction data collected during the first operando experiment (a) and the second in situ experiment (b).

x in Na_xMoO_2	Space group	Cell parameters						$d_{interslab}$ (Å)
		a (Å)	b (Å)	c (Å)	α (°)	β (°)	γ (°)	
0.5[a]	C2/m	4.9337(6)	2.8860(3)	6.1118(1)	90	99.03(1)	90	6.0432
0.593[b]	P-1	4.9420(3)	2.8937(1)	6.3097(3)	90.451(6)	106.996(7)	89.952(6)	6.0342
0.607[b]	P-1	4.9462(4)	2.8946(1)	6.2949(3)	90.481(8)	106.561(7)	89.870(7)	6.0337
0.614[b]	P-1	4.9466(1)	2.8947(1)	6.2946(2)	90.481(4)	106.561(4)	89.870(4)	6.0335
0.634[b]	P-1	4.9455(2)	2.8979(2)	6.2752(2)	90.443(4)	106.381(4)	89.910(4)	6.0204
0.651[b]	P-1	4.9452(2)	2.9005(1)	6.2465(2)	90.384(4)	105.921(5)	89.932(4)	6.0069
0.668[b]	P-1	4.9532(2)	2.9002(1)	6.2494(4)	90.390(3)	106.197(4)	89.887(4)	6.0014
0.688[b]	P-1	4.9539(2)	2.9022(1)	6.2326(2)	90.476(5)	105.971(6)	89.801(5)	5.9920
0.722[b]	P-1	4.9621(2)	2.8991(1)	6.2453(1)	90.454(4)	106.534(4)	89.842(4)	5.9870
0.756[b]	P2/m	4.9688(2)	2.9020(1)	6.2445(2)	90	107.156(4)	90	5.9667
0.82[a]	P2/m	4.9673(3)	2.9021(1)	6.2562(5)	90	108.118(5)	90	5.9478
~0.9[a]	P2/m	4.9966(6)	2.9057(3)	6.2928(9)	90	111.227(8)	90	5.8679

Superstructure peaks in the composition domains $x \approx 0.68$ and $x \approx 0.71$ are presented respectively in **insert A** and **B** of the **Figure 7**, as an example. Furthermore, two types of unindexed peaks with specific peak shapes - broad and thin widths, seem to be distinguishable in several monophasic domains: $x \approx 0.68$ (**Insert A, Figure 7**), $x \approx 0.71$ (**Insert B, Figure 7**) and $0.77 \leq x \leq 0.82$ (**Insert B, Figure 6**). They are believed to arise from two different long-range arrangements in the structure: sodium/vacancy ordering between the $[MoO_2]$ slabs and Mo-Mo bonds patterning in the $[MoO_2]$ slabs. Sodium/vacancy ordering are the result of the partial occupancy of several crystallographic sites by sodium ions to minimize the electrostatic repulsions. As several sites can be occupied by sodium atoms, it is possible to envisage random defects in the long-range, which would lead to a broadening of the resulting superstructure reflections. In contrast, covalent Mo-Mo bonds would be formed through the displacement of molybdenum atoms from an ideal position in the center of the MO_6 octahedra. The patterning of covalent Mo-Mo bonds is therefore thought to be more prone to long distance order than sodium/vacancy ordering and to lead to the appearance of very thin superstructure peaks on the X-ray diffraction patterns.

Monophasic domains are separated from one and other by biphasic domains indicated mainly by the broadening of the 002_t reflection, as the subcell lattice parameters for each specific phase in the x-range $0.58 \leq x \leq 0.72$ are very close. Simultaneously two reflections at higher angle are noted for the same indexation, for example -201_t in the ranges $x \approx 0.65$-0.66 and $x \approx 0.69$. At higher sodium content ($x > 0.75$), biphasic domains are shown as expected by the simultaneous presence of reflections of both phases and with an intensity ratio evolving with sodium content.

Evolution of the cell parameters and stacking

The monoclinic or triclinic subcell parameters were refined using the Le Bail method on each X-ray diffraction pattern acquired during the two *in situ* experiments. Those calculated in monophasic domains are reported in **Table** 1 (Parameters for $Na_{0.55}MoO_2$ are not reported as we could not index its unit cell from our operando experimental diffraction data). Those calculated in biphasic domains are reported in Supporting Information (Figure S2). Interestingly, one can notice that the triclinic distortion, evaluated by the difference from 90° of the values of α and γ angles, is not constant and depends on the sodium content. The lowest distortion occurs for $Na_{0.65}MoO_2$ and the greatest for $Na_{0.69}MoO_2$. The distance between two $[MoO_2]$ slabs called interslab distance ($d_{interslab} = c * \sin\beta$) is reported as well. As expected this distance continuously decreases until $x = 0.82$ as a result from the screening of the electrostatic repulsions between $[MoO_2]$ slabs due to the intercalation of sodium ions in the interslab. For high sodium contents, the screening is even more important and this lead to a greater decrease in the interslab distance, illustrated by the shifts of the *00l* reflections of the $Na_{\sim 0.9}MoO_2$ and Na_1MoO_2 compositions towards higher 2θ angles.

Table 2. Indexation of the reflections in monoclinic cells (O'3 or P'3-type structure) or triclinic cells (O''3 or P''3-type structure) resulting from the splitting of the *104* and *105* reflections in hexagonal cells (O3 or P3-type structure).

Hexagonal	Monoclinic	Triclinic
104_h	-202_m	-202_t
	111_m	111_t
		-111_t
105_h	201_m	201_t
	-112_m	-112_t
		$-1-12_t$

Reliable structural determination using the Rietveld method on (*operando*) *in situ* X-ray diffraction data requires the indexation of the superstructures or modulation peaks that has not been possible yet. Nevertheless, information on the type of site occupied by the sodium ions between the $[MoO_2]$ slabs can still be retrieved. Sodium layered oxides usually adopt two types of stacking, named O3 and P3 according to Delmas nomenclature[38].

In these structures, three $[MO_2]$ slabs are necessary to describe the structure in the common hexagonal cell and sodium ions occupy respectively octahedral and prismatic sites in the interslab space. Transitions from one stacking to another are possible through slab gliding requiring only small atomic displacement and no breaking of M-O bonds. They can therefore occur at room temperature during the cycling of the battery[29,30,39,40], as it was more recently shown in the $O3\text{-}Na_xMn_{1/3}Fe_{2/3}O_2$ system[41]. This difference in stacking arrangements leads to a significant change in intensity ratio between the reflections 104_h and 105_h in the X-ray diffraction patterns indexed with an undistorted hexagonal cell. 104_h reflection is the most intense when sodium has an octahedral coordination and conversely 105_h is the most intense when sodium is in prismatic sites. Monoclinic distortions, indicated in the nomenclature by O'3, P'3, and further triclinic distortions, written O''3 and P''3, induce the splitting of these reflections. The O'3- and P'3 structure types are presented in Figure 8, a and b, respectively. The angles α and γ, deviating slightly from 90° in the triclinic structure are shown in Figure 9c in the P'3-structure type. The resulting splitting of the 104_h and 105_h peaks in monoclinic and triclinic cells are reported **Table 2**.

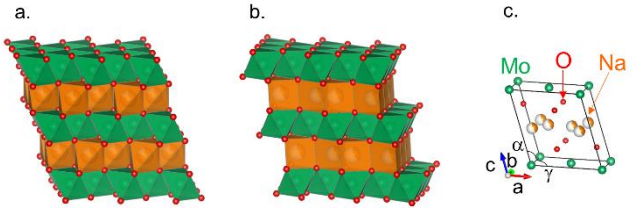

Figure 8. a and b. O'3- and P'3-type structures, respectively. c. Triclinic subcell of the P''3-structure type showing α and γ angles. Sodium partial occupation is represented by partially colored balls.

By following the intensity ratio of the relevant sets of peaks indicated **Table 2** for each system (hexagonal, monoclinic or triclinic) on the *in situ* diffraction data, reliable conclusions on the structural evolution and slab gliding upon sodium intercalation can be drawn. Five X-ray diffraction patterns recorded during the *operando* experiment (x= 0.5, ~0.9) and the *in situ* experiment (x = 0.59, 0.75, 0.77) are presented in **Figure 9** to highlight this slab gliding occurring during the sodium electrochemical intercalation.

Firstly sodium ions occupy octahedral sites in $Na_{0.5}MoO_2$ as it is clear that the 111_m and -202_m reflections are stronger than the 201_m and -112_m ones, in agreement with the model previously reported in the literature[14,24]. The stacking of the next phase, $Na_{0.55}MoO_2$, is still unclear as the subcell indexing its X-ray pattern has not been determined yet. A transition from an O'3 to a P''3 stacking is however believed to happen around the $Na_{0.55}MoO_2$ composition, as the Na_xMoO_2 phases adopt a P"3 type stacking in the triclinic domain, $0.58 < x < 0.75$. In this composition range, the intensity ratio is reverse with weaker 111_t, $1\text{-}11_t$ and -202_t reflections and stronger -112_t, $-1\text{-}12_t$ and 201_t ones. This transition could moreover generate stacking faults during the phase transition and explains the important broadening of the reflections in the composition range $0.5 < x < 0.58$ as indicated previously in this paper. This explanation was recently proposed for the Na_xVO_2 system in which a similar observation was made[13]. Trigonal prismatic coordination for sodium is kept in the monoclinic phases, P'3-$Na_{0.75}MoO_2$ and P'3-$Na_{0.82}MoO_2$. O'3-type stacking is recovered for $Na_{\sim0.9}MoO_2$ with a new intensity inversion with strong 111_m and -202_m reflections and weak 201_m and -112_m ones. The octahedral coordination for sodium is also maintained in Na_1MoO_2. Its structural characterization is in progress, but our preliminary results indicate an octahedral environment for sodium. This transition from P'3 to O'3 could explain the difference of polarization observed at low and high sodium contents, on the GITT curve (**Figure 4**). Indeed, P'3 phases have lower polarization and shorter relaxation times than O'3 phases, due to different diffusion paths of the sodium ions in the structure[42]. Whereas in P'3 phases, sodium crosses a rectangular face, in O'3 phases they pass through an intermediate tetrahedral site and two triangular bottlenecks, involving a greater activation energy.

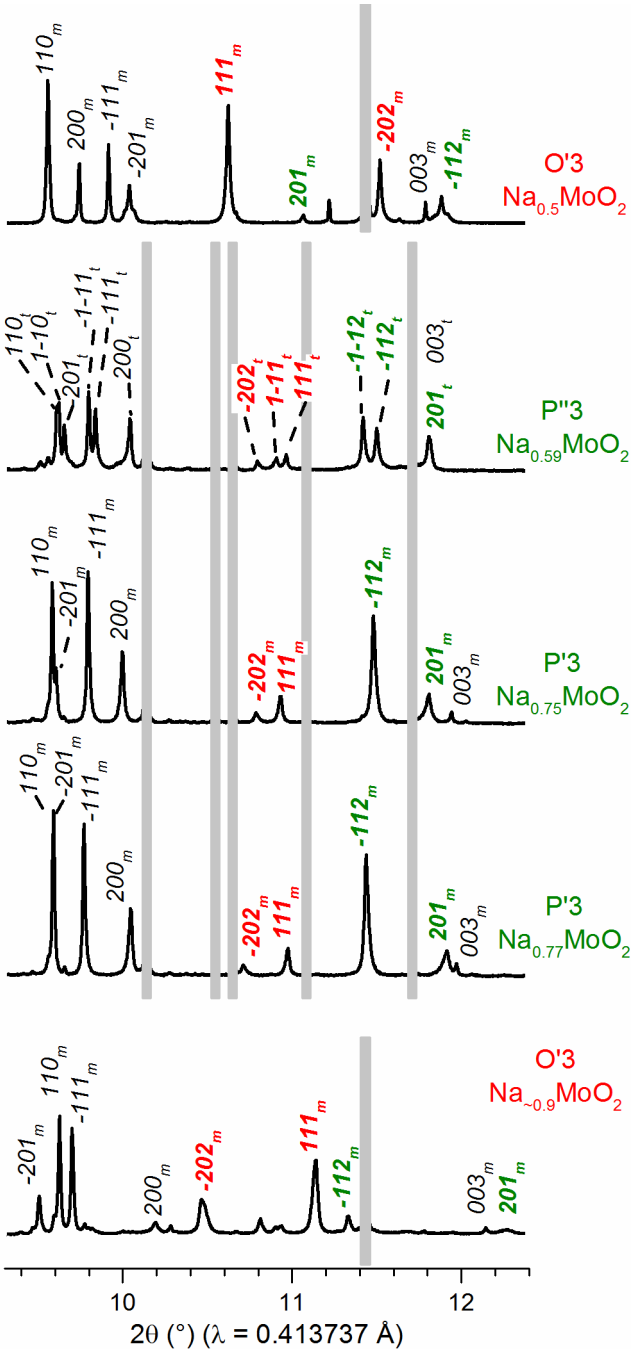

Figure 9. Determination of the stacking type of the structure of the main single phases based on the intensity ratio of reflections issued from 104_{hex} and 105_{hex}. Diffraction from the in situ cells were hidden by grey rectangles.

3. CONCLUSION

The investigation of the Na_xMoO_2 system revealed good reversibility for $0.5 \leq x < 1$. *In situ* synchrotron X-ray diffraction experiments were used to understand the structural origin of the complexity of the electrochemical curve and establish a detailed phase diagram for Na_xMoO_2 system as

shown in **Figure 10.** This figure shows the correlation between the variations observed on the electrochemical curve and the structural transitions evidenced by *in situ* X-ray diffraction. Particularly, thirteen monophasic domains with very close sodium contents have been highlighted. Nine of these domains are characterized by different superstructures and a modulated structure has been shown in the $0.66 \leq x \leq 0.67$ composition domain. They are thought to result from different sodium/vacancy ordering and/or the formation of Mo-Mo bonds arranged in various patterns in the structure of these materials. The latter would also explain the triclinic distortion occurring in the $0.58 \leq x < 0.76$ composition domain and such a distortion has never been evidenced in any other Na_xMO_2 system at room temperature.

Ex situ characterization is necessary to evidence the arrangement of Mo-Mo bonds and/or the sodium/vacancy ordering in the Na_xMoO_2 structures and to understand how they affect the physical properties of the material. Systematic studies by electron diffraction are in progress to characterize the structure of these materials. Electrochemical synthesis has been proven to be a powerful tool to obtain ordered Na_xMO_2 phases[6,10,11], but is particularly challenging in Na_xMoO_2. The very small voltage steps on the electrochemical curve attest to low potential barriers between two consecutive Na_xMoO_2 phases that are therefore easily crossed at room temperature. For now, only $Na_{0.5}MoO_2$ and $Na_{0.66}MoO_2$ were successfully isolated and their characterization is currently under way.

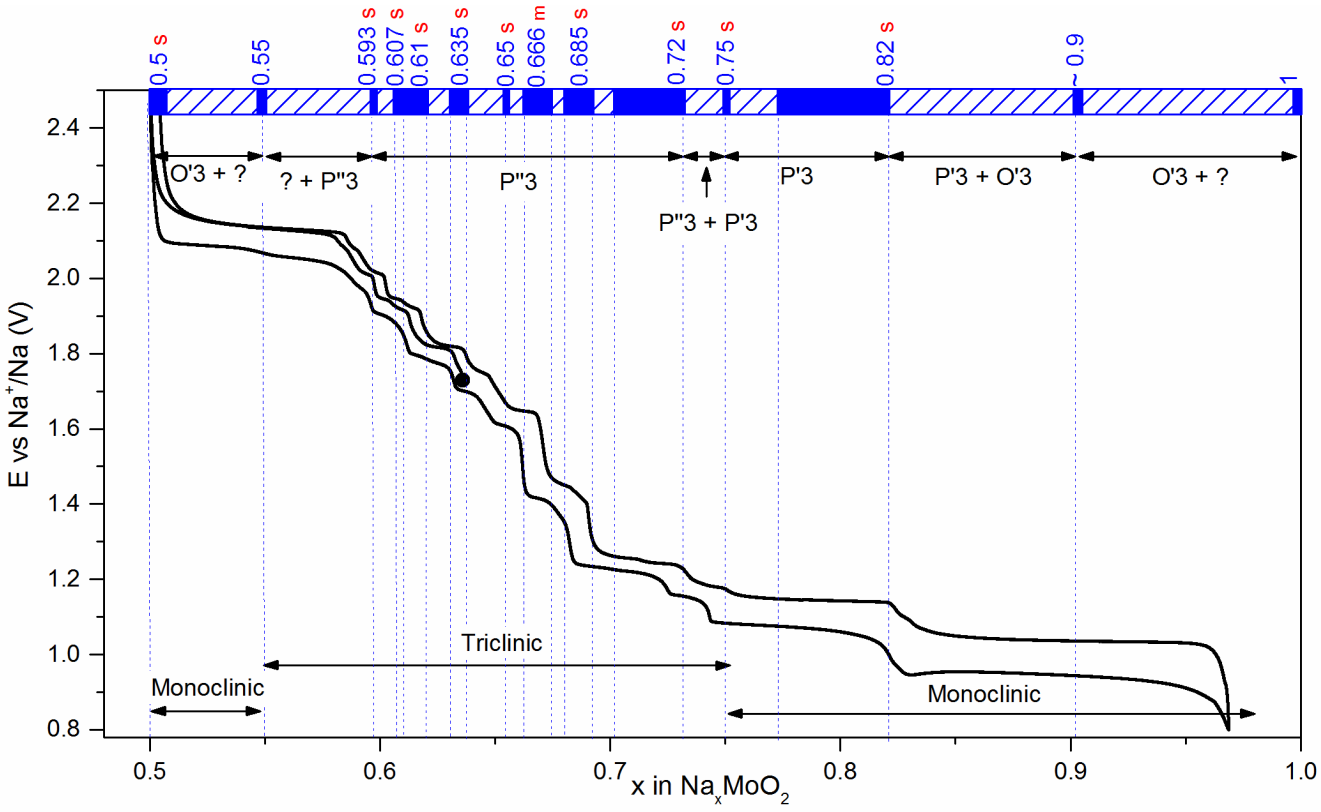

Figure 10. Correlation between the variations observed on the electrochemical curve and the phase diagram determined by in situ X-ray diffraction. A complete phase diagram for the composition range $1/2 \leq x < 1$ is presented on the top : Monophasic domains and biphasic domains are stated respectively by blue and striped areas. Sodium content of each specific phases are written in blue. Superstructures are highlighted by a red « s » and modulated structures by « m ». Symmetry of the cell and the stacking types are also reported on the electrochemical curve.

ASSOCIATED CONTENT

Supporting Information. The enlargement of the X-ray diffraction patterns acquired during the two in situ experiments in the 2θ-ranges displaying the evolution of the diffraction lines issued from 104_{hex} and 105_{hex} upon sodium intercalation can be found in Supporting Information. An evolution of the cell parameters a, b, c, α, β and γ upon sodium intercalation can also be found. This material is available free of charge via the Internet at http://pubs.acs.org.

AUTHOR INFORMATION

Corresponding Author

*marie.guignard@icmcb.cnrs.fr

ACKNOWLEDGMENT

MG would like to thank the Agence Nationale de la Recherche for providing support through the grant ANR-14-CE05-0011. Use of the Advanced Photon Source at Argonne National Laboratory was supported by the U. S. Department of Energy, Office of Science, Office of Basic Energy Sciences, under Contract No. DE-AC02-06CH11357. JCP would like thank UNSW/ANSTO and

AINSE for the PhD Scholarship. NS would like to thank the Australian Research Council for providing support through the DECRA (DE160100237) and DP (DP170100269) programs. Part of this research was undertaken on the Powder Diffraction beamline at the Australian Synchrotron, Victoria, Australia.

REFERENCES

(1) Roger, M.; Morris, D. J. P.; Tennant, D. A.; Gutmann, M. J.; Goff, J. P.; Hoffmann, J.-U.; Feyerherm, R.; Dudzik, E.; Prabhakaran, D.; Boothroyd, A. T.; Shannon, N.; Lake, B.; Deen, P. P. Patterning of Sodium Ions and the Control of Electrons in Sodium Cobaltate. *Nature* **2007**, *445* (7128), 631–634.

(2) Zandbergen, H. W.; Foo, M.; Xu, Q.; Kumar, V.; Cava, R. J. Sodium Ion Ordering in Na_xCoO_2 : Electron Diffraction Study. *Phys. Rev. B* **2004**, *70* (2), 024101-1–024101-8.

(3) Foo, M. L.; Wang, Y.; Watauchi, S.; Zandbergen, H. W.; He, T.; Cava, R. J.; Ong, N. P. Charge Ordering, Commensurability, and Metallicity in the Phase Diagram of the Layered Na_xCoO_2. *Phys. Rev. Lett.* **2004**, *92* (24), 247001-1–247001-4.

(4) Viciu, L.; Bos, J. W. G.; Zandbergen, H. W.; Huang, Q.; Foo, M. L.; Ishiwata, S.; Ramirez, A. P.; Lee, M.; Ong, N. P.; Cava, R. J. Crystal Structure and Elementary Properties of $Na_X CoO_2$ (x = 0.32 , 0.51, 0.6, 0.75, and 0.92) in the Three-Layer $NaCoO_2$ Family. *Phys. Rev. B* **2006**, *73* (17), 174104-1–174104-10.

(5) Alloul, H.; Mukhamedshin, I. R.; Collin, G.; Blanchard, N. Na Atomic Order, Co Charge Disproportionation and Magnetism in Na_xCoO_2 for Large Na Contents. *EPL Europhys. Lett.* **2008**, *82* (1), 17002-p1–17002p6.

(6) Berthelot, R.; Carlier, D.; Delmas, C. Electrochemical Investigation of the P2–Na_xCoO_2 Phase Diagram. *Nat. Mater.* **2011**, *10* (1), 74–80.

(7) Igarashi, D.; Miyazaki, Y.; Kajitani, T.; Yubuta, K. Disorder-Order Transitions in Na_XCoO_2 (X ~ 0.58). *Phys. Rev. B* **2008**, *78* (18), 184112-1–184112-6.

(8) Alloul, H.; Mukhamedshin, I. R.; Platova, T. A.; Dooglav, A. V. Na Ordering Imprints a Metallic Kagomé Lattice onto the Co Planes of $Na_{2/3}CoO_2$. *EPL Europhys. Lett.* **2009**, *85* (4), 47006-p1–47006-p6.

(9) Guignard, M.; Didier, C.; Darriet, J.; Bordet, P.; Elkaïm, E.; Delmas, C. P2-Na_xVO_2 System as Electrodes for Batteries and Electron-Correlated Materials. *Nat. Mater.* **2012**, *12* (1), 74–80.

(10) Didier, C.; Guignard, M.; Darriet, J.; Delmas, C. O'3–$Na_X VO_2$ System: A Superstructure for $Na_{1/2}VO_2$. *Inorg. Chem.* **2012**, *51* (20), 11007–11016.

(11) Guignard, M.; Carlier, D.; Didier, C.; Suchomel, M. R.; Elkaïm, E.; Bordet, P.; Decourt, R.; Darriet, J.; Delmas, C. Vanadium Clustering/Declustering in P2–$Na_{1/2}$ VO_2 Layered Oxide. *Chem. Mater.* **2014**, *26* (4), 1538–1548.

(12) Li, W.; Reimers, J.; Dahn, J. In Situ X-Ray Diffraction and Electrochemical Studies of $Li_{1-x}NiO_2$. *Solid State Ion.* **1993**, *67* (1–2), 123–130.

(13) Didier, C.; Guignard, M.; Suchomel, M. R.; Carlier, D.; Darriet, J.; Delmas, C. Thermally and Electrochemically Driven Topotactical Transformations in Sodium Layered Oxides Na_XVO_2. *Chem. Mater.* **2016,** *28*, 1462–1471.

(14) McCarley, R. E.; Lii, K.-H.; Edwards, P. A.; Brough, L. F. New Extended Clusters in Ternary Molybdenum Oxides. *J. Solid State Chem.* **1985**, *57*, 17–24.

(15) Torardi, C. C.; McCarley, R. E. Sodium Tetramolybdenum Hexoxide ($NaMo_4O_6$). A Metallic Infinite-Chain Polymer Derived by Condensation of Octahedral Clusters. *J. Am. Chem. Soc.* **1979**, *101* (14), 3963–3964.

(16) Torardi, C. C.; McCarley, R. E. Some Reduced Ternary and Quaternary Oxides of Molybdenum. A Family of Compounds with Strong Metal-Metal Bonds. *J. Solid State Chem.* **1981**, *37*, 393–397.

(17) Torardi, C. C.; Calabrese, J. C. Hydrothermal Synthesis of a New Molybdenum Hollandite Containing Tetranuclear Metal-Atom Clusters. X-Ray Crystal Structure of $K_2Mo_8O_{16}$. *Inorg. Chem.* **1984**, *23* (21), 3281–3284.

(18) Lii, K.-H.; McCarley, R. E.; Kim, S.; Jacobson, R. A. Synthesis and Structure of Ternary Molybdenum Oxides MMo_8O_{10} (M = Li or Zn) Having Orthogonal Nonintersecting Octahedral Cluster Chains. *J. Solid State Chem.* **1986**, *64* (3), 347–358.

(19) Barrier, N.; Tortelier, J.; Gougeon, P. A New Reduced Molybdenum Oxide with a Hollandite-Type Structure, $PrMo_6O_{12}$. *Acta Crystallogr. Sect. E Struct. Rep. Online* **2001**, *57* (1), i3–i5.

(20) Tortelier, J.; McCarroll, W. H.; Gougeon, P. Synthesis, Crystal Structure, and Characterization of the New Ordered Hollandite-Type $NdMo_6O_{12}$. *J. Solid State Chem.* **1998**, *136* (1), 87–92.

(21) Hubert, P.-H. On the Synthesis of Sodium Molybdenum Oxide. *Compte Rendus Académie Sci. Paris Sér. C* **1966**, 262, 1189-1191.

(22) Reau, J.-M.; Fouassier, C.; Hagenmuller, P. The Systems MoO_2-A_2O et WO_2-A_2O (A = Li,Na,K). *Bull. Société Chim. Fr.* **1970**, *11* (619), 3827–3829.

(23) Hirano, S.; Kozima, M.; Naka, S. Hydrothermal Synthesis and Properties of Na_xMoO_2 Single Crystal. *Toyota Kenkyu Hokoku* **1984**, *37*, 32–38.

(24) Tarascon, J. M.; Hull, G. W. Sodium Intercalation into the Layered Oxides $Na_xMo_2O_4$. *Solid State Ion.* **1986**, *22*, 85–96.

(25) Burdett, J. K.; Hughbanks, T. Aspects of Metal-Metal Bonding in Early-Transition-Metal Dioxides. *Inorg. Chem.* **1985**, *24* (12), 1741–1750.

(26) Ringenbach, C.; Kessler, H.; Hatterer, A. A New Molyldenum Oxide $NaMoO_2$. Crystallographic and Magnetic Properties. *Compte Rendus Séances Académie Sci. Sér. C* **1969**, *269*, 1394–1397.

(27) Petříček, V.; Dušek, M.; Palatinus, L. Crystallographic Computing System JANA2006: General Features. *Z. Für Krist. - Cryst. Mater.* **2014**, *229* (5), 345–352.

(28) Parant, J.-P.; Olazcuaga, R.; Devalette, M.; Fouassier, C.; Hagenmuller, P. On Some New Phases with the Formula Na_xMnO_2 (X⩽ 1). *J. Solid State Chem.* **1971**, *3* (1), 1–11.

(29) Fouassier, C.; Matejka, G.; Reau, J.-M.; Hagenmuller, P. On New Oxide Bronzes with the Formula Na_xCoO_2 (X<l). The System Cobalt-Oxygen-Sodium. *J. Solid State Chem.* **1973**, *6*, 532–537.

(30) Braconnier, J.-J.; Delmas, C.; Hagenmuller, P. Study by Electrochemical Deintercalation of the Systems Na_xCrO_2 and Na_xNiO_2. *Mater. Res. Bull.* **1982**, *17*, 993–1000.

(31) Takeda, Y.; Nakahara, K.; Nishijima, M.; Imanishi, N.; Yamamoto, O.; Takano, M. Sodium Deintercalation from Sodium Iron Oxide. *Mater. Res. Bull.* **1994**, *29* (6), 659–666.

(32) Szajwaj, O.; Gaudin, E.; Weill, F.; Darriet, J.; Delmas, C. Investigation of the New P'3-Na $_{0.60}$ VO_2 Phase: Structural and Physical Properties. *Inorg. Chem.* **2009**, *48* (19), 9147–9154.

(33) Han, M. H.; Gonzalo, E.; Casas-Cabanas, M.; Rojo, T. Structural Evolution and Electrochemistry of Monoclinic $NaNiO_2$ upon the First Cycling Process. *J. Power Sources* **2014**, *258*, 266–271.

(34) Komaba, S.; Nakayama, T.; Ogata, A.; Shimizu, T.; Takei, C.; Takada, S.; Hokura, A.; Nakai, I. Electrochemically Reversible Sodium Intercalation of Layered $NaNi_{0.5}Mn_{0.5}O_2$ and $NaCrO_2$; ECS, 2009; pp 43–55.

(35) Hamani, D.; Ati, M.; Tarascon, J.-M.; Rozier, P. Na_xVO_2 as Possible Electrode for Na-Ion Batteries. *Electrochem. Commun.* **2011**, *13* (9), 938–941.

(36) Lee, D. H.; Xu, J.; Meng, Y. S. An Advanced Cathode for Na-Ion Batteries with High Rate and Excellent Structural Stability. *Phys. Chem. Chem. Phys.* **2013**, *15* (9), 3304–3312.

(37) Lang, G.; Bobroff, J.; Alloul, H.; Collin, G.; Blanchard, N. Spin Correlations and Cobalt Charge States: Phase Diagram of Sodium Cobaltates. *Phys. Rev. B* **2008**, *78* (15) 155116-1–155116-12.

(38) Delmas, C.; Fouassier, C.; Hagenmuller, P. Structural Classification and Properties of the Layered Oxides. *Physica* **1980**, *99B*, 81–85.

(39) Delmas, C.; Braconnier, J.-J.; Fouassier, C.; Hagenmuller, P. Electrochemical Intercalation of Sodium in Na_xCoO_2 Bronzes. *Solid State Ion.* **1981**, *3/4*, 165–169.

(40) Mendiboure, A.; Delmas, C.; Hagenmuller, P. Electrochemical Intercalation and Deintercalation of Na_xMnO_2 Bronzes. *J. Solid State Chem.* **1985**, *57*, 323–331.

(41) Mortemard de Boisse, B.; Cheng, J.-H.; Carlier, D.; Guignard, M.; Pan, C.-J.; Bordère, S.; Filimonov, D.; Drathen, C.; Suard, E.; Hwang, B.-J.; Wattiaux, A.; Delmas, C. O3–Na_x $Mn_{1/3}Fe_{2/3}O_2$ as a Positive Electrode Material for Na-Ion Batteries: Structural Evolutions and Redox Mechanisms upon Na^+ (De)intercalation. *J Mater Chem A* **2015**, *3* (20), 10976–10989.

(42) Delmas, C.; Maazaz, A.; Fouassier, C.; Réau, J.-M.; Hagenmuller, P. Influence of the environment of alcaline ion on its mobility in layered $A_x(L_xM_{1-x})O_2$. *Mater. Res. Bull.* **1979**, *14* (3), 329–335.